Int. J. Heat Mass Transfer. Vol. 36, No. 8, pp. 2193–2202, 1993
Printed in Great Britain

0017–9310/93 $6.00 + 0.00

A theoretical investigation of acoustic enhancement of heat and mass transfer—II. Oscillating flow with a steady velocity component

MAN YEONG HA
Department of Mechanical & Production Engineering, The Pusan National University, 30 Jangjeon-Dong, Kumjung-Ku, Pusan 609-735, Korea

and

SAVASH YAVUZKURT
Department of Mechanical Engineering, The Pennsylvania State University, University Park, PA 16802, U.S.A.

(*Received* 25 *June* 1990 *and in final form* 7 *July* 1992)

Abstract—In order to study the effects of high intensity acoustic fields superposed on a steady flow on heat and mass transfer around spherical particles, a two-dimensional, unsteady computer code which employs the two-dimensional, unsteady conservation of mass, momentum and energy equations for laminar flow in spherical coordinates has been developed. Numerical solutions of these equations give the velocity and temperature fields around the particle for acoustically oscillating flow as a function of acoustic Reynolds number, Strouhal number, and the ratio of the acoustic velocity to the steady slip velocity between the particles and the main flow. The present results show about 85% increase in the space- and time-averaged quasi-steady Nusselt number normalized by its steady value when the ratio of the acoustic velocity to the steady slip velocity is about 5. About 10% decrease in heat transfer is obtained when the ratio of the acoustic velocity to the steady slip velocity is about 1. The space- and time-averaged Nusselt numbers have different values for frequencies of 50, 1000 and 2000 Hz due to the combined effects of the curvature, flow acceleration and flow separation. The maximum difference is about 10%. The results demonstrate a definite enhancement of heat and mass transfer in the presence of high intensity acoustic fields particularly for the case of low steady slip velocity.

INTRODUCTION

THE EFFECT of an oscillating flow field with and without a steady component on heat and mass transfer from single spherical particles and droplets has been a topic of investigation since the late 1930s [1]. Some examples of these theoretical and experimental studies can be found in refs. [2–6]. These publications report an increase, decrease or unnoticeable change in heat and mass transfer, depending on the frequency and the magnitude of the steady and oscillating flow. Zinn *et al.* [7] and Faeser [8] indicate the positive effects of high intensity acoustics on coal combustion by using acoustic drivers or pulsed combustion. Koopmann *et al.* [9] investigated the effects of high intensity acoustic fields on the rate of combustion of coal–water slurry fuel in the sonic combustor. Yavuzkurt *et al.* [10, 11] calculated a decrease of 15.7 and 12.1%, respectively, in the char burn-out length for a sound pressure level of 160 dB and at a frequency of 2000 Hz compared to the case with no sound for the combustion of 100 μm pulverized coal or coal–water slurry fuels.

The previous studies generally concentrated on experimental aspects showing the global effect of oscillating flow field on heat and mass transfer and combustion. There are no detailed theoretical studies investigating the fundamental aspects of this problem in order to understand the governing mechanisms. One reason for this is the very complex nature of the problem at hand. For example, interaction of the acoustic field with the gas field, nonlinear acoustic effects such as wave steepening and shock wave formation, standing waves, and absorption of acoustic energy by the gas and particles all add to the complexity of the problem. The flow field created by the acoustic field is unsteady and in some cases contain the very high frequency. In order to capture the effects of high frequencies a very short time step is needed in numerical calculations. This leads to enormous computational time. The Reynolds number range based on acoustic velocity is very high compared to the Stoke's flow regime and very low for boundary layer assumptions to be valid. Considering these complexities the main objective of this study is to emphasize fundamental aspects in order to investigate the effects of acoustic fields on heat and mass transfer to and from solid and droplet fuels such as pulverized coal and coal–water slurry fuels. This study is fundamental but at the same time it is comprehensive.

NOMENCLATURE

D	diameter
f	frequency
h_0	local heat transfer coefficient
i	static enthalpy
k	thermal conductivity
L_p	sound pressure level
Nu	Nusselt number
P	pressure
Pr	Prandtl number
r	radial position
R	radius of particle
Re_0	steady Reynolds number, $(U_0 D/\nu)$
Re_1	acoustic Reynolds number, $(U_1 D/\nu)$
S	Strouhal number
S_ϕ	source term for general variable ϕ
Sc	Schmidt number
Sh	Sherwood number
SPL	sound pressure level
t	time
T	temperature, period
u_r	radial velocity
u_θ	axial velocity
U_0	steady slip velocity
U_1	acoustic peak velocity.

Greek symbols

Γ_ϕ	diffusivity for general variable ϕ
δ	boundary layer thickness
ε_ϕ	convergence criteria
ε	velocity ratio
θ	angular direction
μ	viscosity
ρ_g	gas density
τ	dimensionless time (tf or t/T)
ϕ	general variable given in equation (1)
ω	angular frequency.

Subscripts

f	oscillating flow
g	gas
h	hydraulic
new	new values
old	old values
p	particle
r	radial
s	space-averaged, surface, separation
t	space- and time-averaged
0	steady, initial
1	acoustic
θ	angular
ϕ	dependent variables
∞	infinity.

In the initial stage of combustion of pulverized coal or coal–water slurry droplets, there exists a steady slip velocity, U_0, before coal particles or particle agglomerates become entrained in the main gas flow. In order to consider the effects of this steady slip velocity, an oscillating flow, $U_1 \cos(2\pi t/T)$, induced by the longitudinal, high intensity acoustic fields is superposed on the mean steady flow, U_0, in the present study. This paper presents a theoretical and computational study of the effects of high intensity fields on the heat and mass transfer. In order to study these phenomena, a two-dimensional, unsteady computer code has been developed. This is used to solve the two-dimensional, unsteady conservation of mass, momentum and energy equations for a laminar flow in spherical coordinates. The effects of varying acoustic Reynolds number, Strouhal number and ratio of the acoustic peak velocity to the steady slip velocity on heat and mass transfer to and from a single particle are investigated.

GOVERNING EQUATIONS AND BOUNDARY CONDITIONS

The hydrodynamic and thermal characteristics of an oscillating flow created by an acoustic field over a single particle are studied by solving the unsteady and two-dimensional axisymmetric conservation equations for constant property, laminar flow with the following common form (see Patankar [12]):

$$\frac{\partial}{\partial t}(\rho\phi)+\frac{1}{r^2}\frac{\partial}{\partial r}(r^2\rho u_r\phi)+\frac{1}{r\sin\theta}\frac{\partial}{\partial\theta}(\sin\theta\,\rho u_\theta\phi)=\frac{1}{r^2}\frac{\partial}{\partial r}\left(\Gamma_\phi r^2\frac{\partial\phi}{\partial r}\right)+\frac{1}{r^2\sin\theta}\frac{\partial}{\partial\theta}\left(\Gamma_\phi\sin\theta\frac{\partial\phi}{\partial\theta}\right)+S_\phi. \quad (1)$$

The flow field and the particle geometry with some nomenclature are shown in Fig. 1. In the conservation of momentum equation, $\phi = u_r, u_\theta$ represents the velocities in the radial r and axial θ directions, respectively. In the energy equation $\phi = i$ is the static enthalpy. The source terms S_ϕ in equation (1) are given in Table 1. The quantities are allowed to vary in the radial (r) and axial (θ) directions whereas a circumferential symmetry is assumed around an axis which passes through the center of the particle and is parallel to the flow direction.

The governing equation (1) has the following initial and boundary conditions:

Initial conditions ($t = 0$):

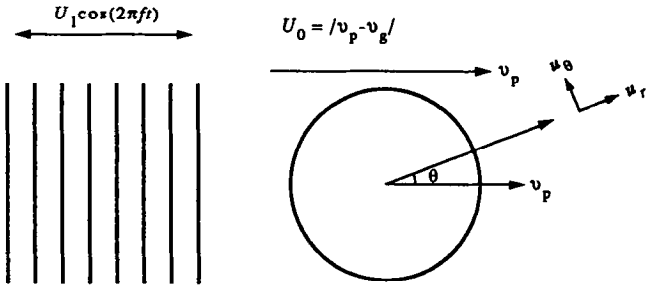

FIG. 1. Schematic diagram showing the geometry and some of the nomenclature used to simulate heat and mass transfer from a spherical particle in the presence of a high intensity acoustic field.

$$\phi = \phi_0 \tag{2}$$

Boundary conditions ($t > 0$):

$$\frac{\partial \phi}{\partial \theta} = 0, \quad \text{at } \theta = 0 \text{ and } \pi \text{ (Symmetry conditions)} \tag{3}$$

$$\phi = \phi_p, \quad \text{at } r = R \tag{4}$$

and as $r \to \infty$,

$$u_\theta = -[U_0 + U_1 \cos(2\pi t/T)] \sin\theta$$
$$u_r = [U_0 + U_1 \cos(2\pi t/T)] \cos\theta$$
$$i = i_\infty. \tag{5}$$

In equations (4) and (5), ϕ_p represents the value of the dependent variable ϕ at the particle surface, U_0 is the steady component of the flow velocity with respect to the particles and U_1 is the peak value of the acoustic velocity. The present study considers only the case of a longitudinal acoustic field. Thus the steady velocity, U_0, and acoustic velocity, $U_1 \cos(2\pi t/T)$, are co-linear. The velocities u_{rp} and $u_{\theta p}$ in equation (4) are zero. The static enthalpy i_p is a constant value determined by a specified particle temperature.

The conservation equations given by equation (1) with the above initial and boundary conditions are solved using a finite difference method with 30 grid points in the θ and 50 in the r direction. The numerical solution for the algebraic equations of equation (1) is obtained using the SIMPLEC algorithm of Van Doormaal and Raithby [13] (see Ha [14] for more detailed discussions), giving the velocity and temperature fields for oscillating flow over a spherical particle as a function of time. From the calculated temperature distribution, the local Nusselt number, Nu_θ, is calculated as

$$Nu_\theta = \frac{h_\theta D}{k} = \frac{D}{(T_p - T_\infty)} \left.\frac{\partial T}{\partial r}\right|_{r=R}. \tag{6}$$

Integrating the local Nusselt number in the axial direction, the space-averaged Nusselt number, Nu_s, is obtained. This is given by the following equation:

$$Nu_s = \frac{1}{\pi} \int_0^\pi Nu_\theta \, d\theta. \tag{7}$$

After the steady periodic state is reached, meaning that the space-averaged Nusselt number over a cycle is the same as the value obtained in the following cycles, the space- and time-averaged, quasi-steady Nusselt number, Nu_t, is calculated as follows:

$$Nu_t = \frac{1}{T} \int_0^T Nu_s \, dt \tag{8}$$

Table 1. Source terms S_ϕ used in equation (1)

ϕ	Γ_ϕ	S_ϕ
1	0	0
u_r	μ	$-\frac{\partial p}{\partial r} + \frac{1}{r^2}\frac{\partial}{\partial r}\left(\mu r^2 \frac{\partial u_r}{\partial r}\right) + \frac{1}{r\sin\theta}\frac{\partial}{\partial\theta}\left(\mu \sin\theta \frac{\partial u_\theta}{\partial r}\right) - \frac{1}{r^2\sin\theta}\frac{\partial}{\partial\theta}(\mu \sin\theta u_\theta) - \frac{2\mu}{r^2}\frac{\partial u_\theta}{\partial\theta} - 4\mu\frac{u_r}{r^2}$ $-2\mu\frac{u_\theta \cot\theta}{r^2} + \rho\frac{u_\theta}{r^2}$
u_θ	μ	$-\frac{1}{r}\frac{\partial p}{\partial\theta} + \frac{1}{r^2}\frac{\partial}{\partial r}\left(\mu r^2 \frac{\partial u_\theta}{\partial r}\right) + \frac{1}{r^2\sin\theta}\frac{\partial}{\partial\theta}\left(\mu\sin\theta\frac{\partial u_\theta}{\partial\theta}\right) + \frac{2}{r\sin\theta}\frac{\partial}{\partial\theta}\left(\mu\sin\theta\frac{u_r}{r}\right) + \frac{\mu}{r}\frac{\partial u_\theta}{\partial r} + \frac{\mu}{r^2}\frac{\partial u_r}{\partial\theta} - \mu\frac{u_\theta}{r^2}$ $-2\mu\frac{u_r\cot\theta}{r^2} - 2\mu\frac{u_\theta\cot^2\theta}{r^2} - \frac{1}{r^2}\frac{\partial}{\partial r}(\mu r u_\theta) - \rho\frac{u_r u_\theta}{r^2}$
i	k/c_p	0

where T represents the period of the applied acoustic field. The important nondimensional parameters in the calculation of the space- and time-averaged, quasi-steady heat and mass transfer coefficients (Nu_t or Sh_t) without chemical reactions are:

Re_0: Reynolds number based on steady slip velocity U_0
$Pr(Sc)$: Prandtl (or Schmidt) number
$S(=fD/U_1)$: Strouhal number
$\varepsilon(=U_1/U_0$ or $Re_1/Re_0)$: Velocity ratio.

RESULTS AND DISCUSSION

The steady velocity (U_0), the amplitude of the oscillating velocity (U_1) and the frequency (f) of the applied acoustic field are varied in order to obtain the values of the Nusselt and Sherwood numbers for different steady and acoustic Reynolds and Strouhal numbers. The steady Reynolds numbers, Re_0, which are taken into consideration are 6.3 ($U_0 = 1.0\ \mathrm{m\ s^{-1}}$) and 31.5 ($U_0 = 5.0\ \mathrm{m\ s^{-1}}$). For these steady Reynolds numbers, the acoustic Reynolds number, Re_1, is varied giving an $\varepsilon\ (=Re_1/Re_0)$ between 0.5 and 10.0. The Strouhal numbers S are in the range of 0.0002–0.4. For these small values of Strouhal number, the velocity and temperature fields reach steady periodic state at an early time. Thus the following discussion concentrates on the results over one cycle after reaching a steady periodic state, unless it is mentioned otherwise.

Figures 2 and 3 show the constant temperature lines in the domain from R to $8R$ for $Re_0 = 31.5$ and for $Re_1 = 31.5$ at 50 and 2000 Hz ($S = 0.001$ and 0.04). For the case $Re_0 \geqslant Re_1$, the flow direction is always from left to right and higher temperature gradients are observed around the leading half of the sphere, particularly near the stagnation point ($\theta = 180$), resulting in high heat transfer rates in this region. When $Re_1 > Re_0$ the stagnation point associated with high heat transfer rates is changed with the changing flow direction as explained by Ha [14]. The constant temperature lines for $Re_0 = 31.5$ and for Reynolds numbers of 15.7 and 94.4 at 50 and 2000 Hz ($S = 0.00033$–0.08) are shown by Ha [14].

Figures 4–6 show the local Nusselt number variation with angle for $Re_0 = 31.5$ and for Reynolds numbers Re_1 of 15.7, 31.5 and 94.4 over one cycle between $\tau = 0.0$ and 1.0 at frequencies of 50 and 2000 Hz. As shown in Fig. 4, when $Re_0 = 31.5$ and $Re_1 = 15.7$, the local Nusselt number, $Nu_\theta - 2$, has a maximum value at the stagnation point of $\theta = 180.0$ and decreases along the stream-wise direction ($\theta = 180.0 \rightarrow \theta = 0.0$). The magnitude of $Nu_\theta - 2$ decreases with the decreasing magnitude of the oscillating velocity U during the half cycle from $\tau = 0.0$ to 0.5 and increases with increasing U during the half cycle from $\tau = 0.5$ to 1.0. When $Re_0 = 31.5$ and $Re_1 = 15.7$, the magnitude of the oscillating flow velocity U is the main factor and the flow acceleration of the free stream makes a smaller contribution to $Nu_\theta - 2$. Therefore, the values of $Nu_\theta - 2$ at frequencies of 50 and 2000 Hz are almost the same.

When Re_1 increases to 31.5 ($Re_0 = Re_1$), $Nu_\theta - 2$ has a similar shape to the case of $Re_0 = 31.5$ and

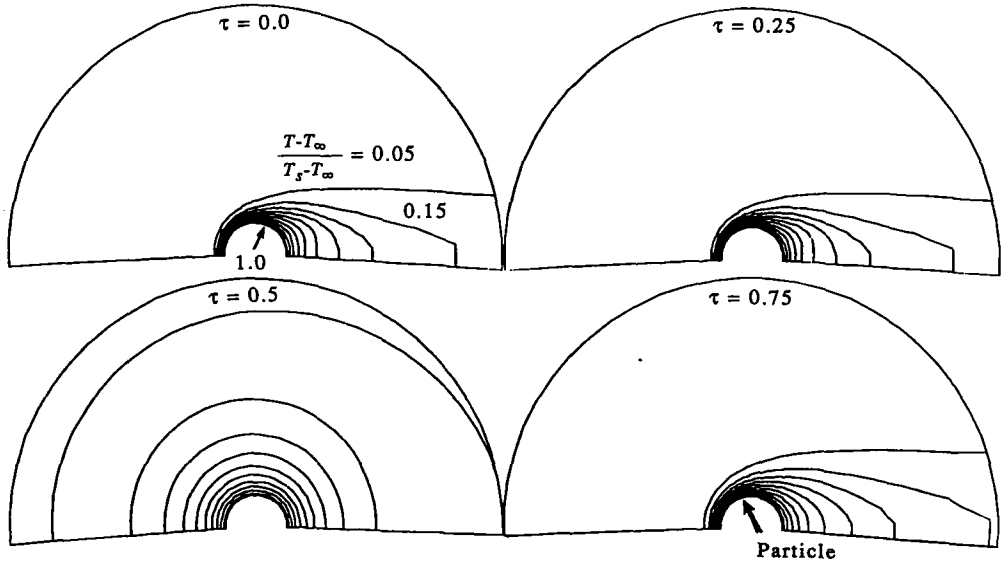

FIG. 2. Constant temperature lines due to an acoustic field with $SPL = 157$ dB superposed on a steady flow around a spherical particle of diameter 100 μm at different times during one cycle: $Re_0 = 31.5$, $Re_1 = 31.5$, $S = 0.001$ ($f = 50$ Hz).

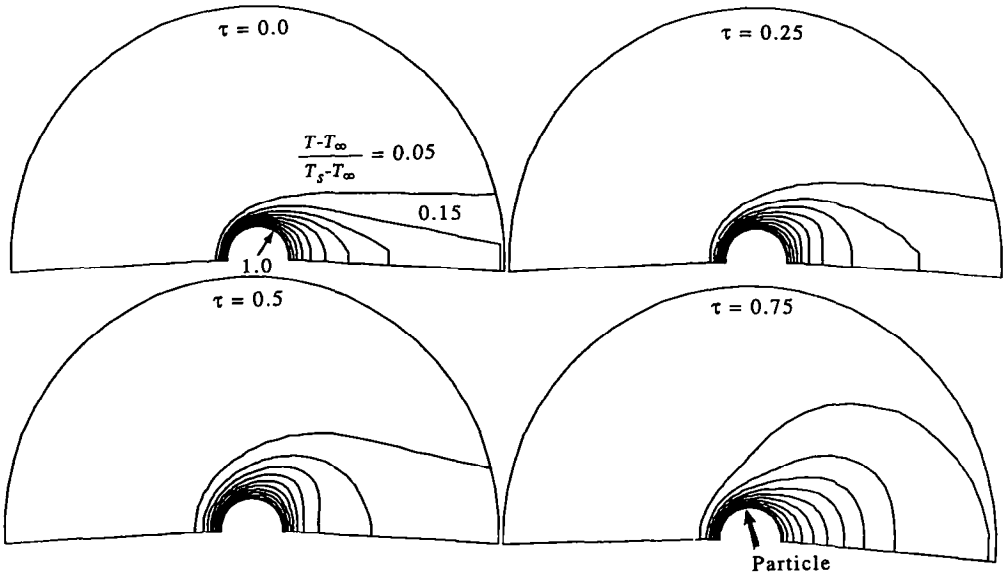

FIG. 3. Constant temperature lines due to an acoustic field with $SPL = 157$ dB superposed on a steady flow around a spherical particle of diameter 100 μm at different times during one cycle: $Re_0 = 31.5$, $Re_1 = 31.5$, $S = 0.04$ ($f = 2000$ Hz).

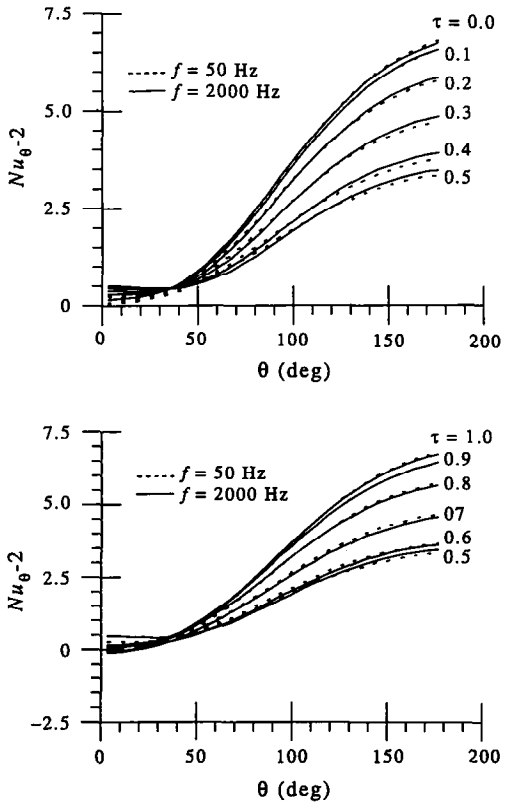

FIG. 4. Angular variation of local Nusselt number due to an acoustic field with $SPL = 151$ dB for frequencies of 50 Hz ($S = 0.002$) and 2000 Hz ($S = 0.08$) around a spherical particle of diameter 100 μm at different times during one cycle: $Re_0 = 31.5$, $Re_1 = 15.7$.

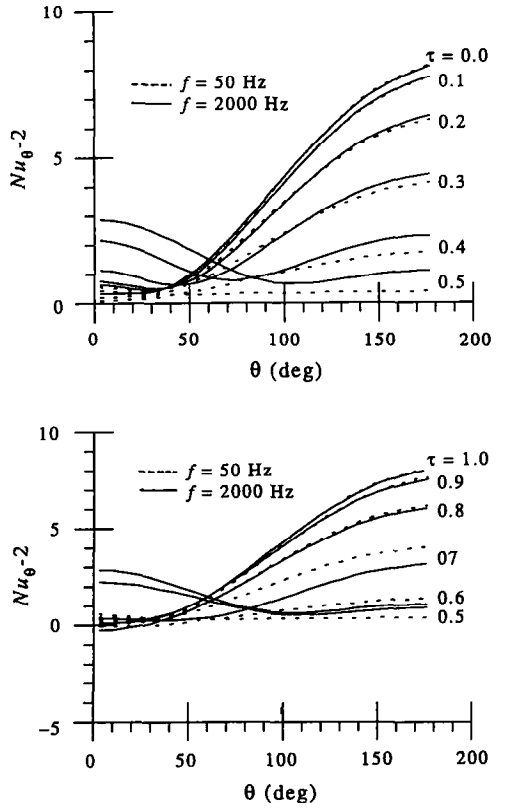

FIG. 5. Angular variation of local Nusselt number due to an acoustic field with $SPL = 157$ dB for frequencies of 50 Hz ($S = 0.001$) and 2000 Hz ($S = 0.04$) around a sphere particle of diameter 100 μm at different times during one cycle: $Re_0 = 31.5$, $Re_1 = 94.4$.

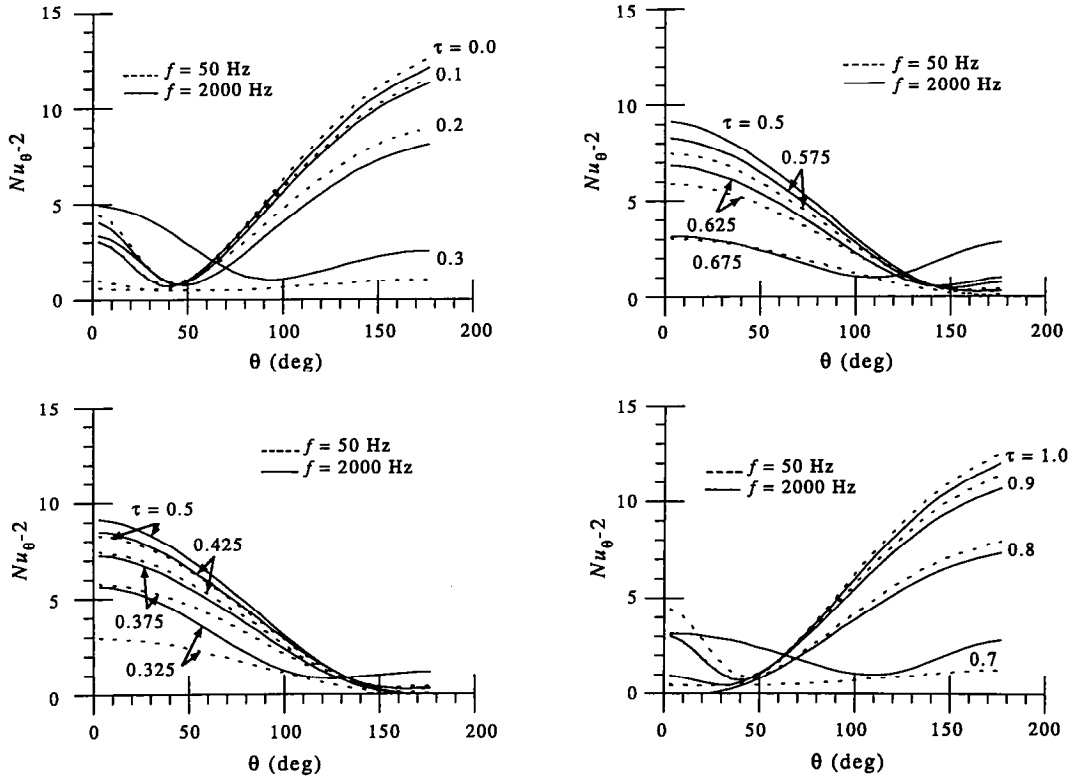

FIG. 6. Angular variation of local Nusselt number due to an acoustic field with $SPL = 167$ dB for frequencies of 50 Hz ($S = 0.0003$) and 2000 Hz ($S = 0.0133$) around a spherical particle of diameter 100 μm at different times during one cycle: $Re_0 = 31.5$, $Re_1 = 94.4$.

$Re_1 = 15.7$ at 50 Hz over one cycle, as shown in Fig. 5. The values of $Nu_\theta - 2$ at 2000 Hz are almost the same as those at 50 Hz during $\tau = 0.0$ to 0.3 and from 0.8 to 1.0 since the major variable affecting heat transfer is the magnitude of the oscillating velocity U. At dimensionless times of 0.4–0.5, the flow causes increasing separation and induces a flow from left to right along the sphere surface as shown by Ha [14]. Therefore, the values of $Nu_\theta - 2$ at 2000 Hz are higher than those at 50 Hz at $\tau = 0.4$ and 0.5. During $\tau = 0.5$–0.7, this induced flow on the surface from the previous period ($\tau = 0.4$–0.5) has an opposite direction with respect to U and decreases the velocity near the surface compared to the case of 50 Hz. Thus, this reverse flow reduces the effect of the favorable pressure gradient, which is a result of flow acceleration during $\tau = 0.5$–0.7, resulting in lower values of $Nu_\theta - 2$ at 2000 Hz around the leading half ($\theta = 180$–90) compared to those at 50 Hz. During $\tau = 0.8$–1.0, the value of the oscillating velocity U is high enough so that the effect of the reverse flow formed previously can be neglected. Thus the favorable pressure gradient due to flow acceleration of the oscillating flow becomes dominant in this period, resulting in almost the same values of $Nu_\theta - 2$ for the low and high frequencies.

When the acoustic Reynolds number Re_1 increases to 94.4 ($Re_1 > Re_0$), the flow acceleration has a more pronounced effect compared to the case of $Re_1 = 15.7$ and 31.5. As discussed in the case of oscillating flow without the steady component by Ha [14], the time delay between the oscillating flow and the thermal boundary layer response causes a decrease in the high values of Nu_θ and an increase in the low ones. During $\tau = 0.0$–0.325 and 0.5–0.675, the flow acceleration of the oscillating flow forms an adverse pressure gradient in the stream-wise direction, resulting in flow separation and inducing a reverse flow which has the same direction as the oscillating flow U in the following period from $\tau = 0.325$–0.5 and from 0.675–1.0. This reverse flow increases with increasing frequency and causes an increase in the high and low values of Nu_θ. During the time from $\tau = 0.0$–0.2, the decreased favorable pressure gradient in the upstream region due to flow acceleration at 2000 Hz gives a lower $Nu_\theta - 2$ for 2000 Hz than that of 50 Hz, as shown in Fig. 6. At $\tau = 0.3$, a reverse flow along the surface exists even though the oscillating flow at infinity is from left to right as shown by Ha [14], resulting in the increased values of $Nu_\theta - 2$ at 2000 Hz compared to those at 50 Hz. During $\tau = 0.325$–0.5, the reverse flow formed during the previous period ($\tau = 0.0$–0.3) and the favorable pressure gradient in the stream-wise direction due to flow acceleration have complementary effects, giving higher values of $Nu_\theta - 2$ at 2000 Hz than at 50 Hz. During $\tau = 0.5$–0.675, the reverse flow and the adverse pressure gradient due to

flow acceleration have opposite effects. However, the values of $Nu_\theta - 2$ at 2000 Hz are still higher than those at 50 Hz. The values of $Nu_\theta - 2$ during this time period are smaller than those during $\tau = 0.325$–0.5 due to the difference in the combined effect of curvature and the axial pressure gradient caused by acceleration of the oscillating flow. Around $\tau = 0.7$, reverse flow ($\theta = 180 \rightarrow 0$) is formed along the surface. The magnitude of the reverse flow at $\tau = 0.7$ is less than that at $\tau = 0.3$, as shown by Ha [14], since the time of exposure to the adverse pressure gradient caused by flow acceleration at infinity during $\tau = 0.5$–0.7 is shorter than that during $\tau = 0.0$–0.3 and the magnitude of the pressure gradient during $\tau = 0.5$–0.7 is smaller than that during $\tau = 0.0$–0.3. This reverse flow causes an increase in the values of $Nu_\theta - 2$ at 2000 Hz compared to those at 50 Hz. Since the reverse flow formed around $\tau = 0.7$ is small compared to the case of $Re_0 = 0.0$ and $Re_1 = 94.4$, the time delay between the acoustic field and the thermal boundary layer response is the major factor determining the values of $Nu_\theta - 2$, giving a slightly lower value of $Nu_\theta - 2$ at 2000 Hz than at 50 Hz during the time from 0.8 to 1.0.

Figure 7(a) shows the space-averaged Nusselt number ($Nu_s - 2$) as a function of dimensionless time τ for the oscillating flow with steady Reynolds number $Re_0 = 31.5$ and acoustic Reynolds numbers ranging from 0 to 94.4. The normalized velocity (U/U_0) of the acoustic field is shown in Fig. 7(b). The Strouhal number is varied in the range 0.008–0.08. An increase

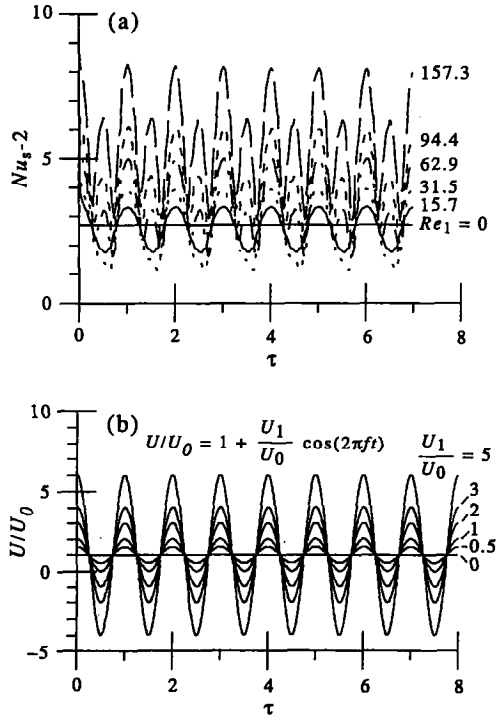

FIG. 7. (a) Space-averaged Nusselt number as a function of τ for $S = 0.008$–0.08 at acoustic Reynolds numbers in the range 0–157.3 (SPL = 0–171 dB) and (b) the applied acoustic field superposed on a steady flow ($Re_0 = 31.46$).

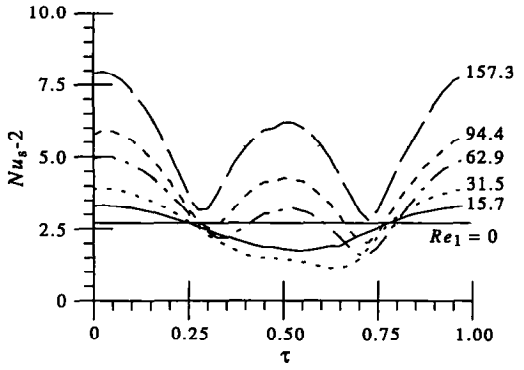

FIG. 8. Quasi-steady space-averaged Nusselt number during a cycle: $S = 0.008$–0.08, $Re_0 = 31.5$, $Re_1 = 0$–157.3 (SPL = 0–171 dB).

in the $Nu_s - 2$ and the magnitude of the oscillations is observed with increasing acoustic Reynolds number. Figure 7 also includes the value of $Nu_s - 2$ when there is no oscillating flow ($U_1 = 0$). The quasi-steady space-averaged Nusselt numbers are shown in Fig. 8 over one cycle after the steady periodic state is reached. As shown in Figs. 7 and 8, when the magnitude of the applied acoustic velocity is less than that of the steady velocity (i.e. $U_1 < U_0$ or $Re_1 < Re_0$), $Nu_s - 2$ shows the same cyclic behavior as the sinusoidal acoustic velocity. However, if U_1 is greater than U_0 ($Re_1 > Re_0$), another high peak at the half time of the period in each cycle is observed. This peak is lower than the highest peak at each period. The figure also indicates that two low peaks are observed at times when $(U_0 + U_1 \cos 2\pi\tau) = 0$ for the case of $U_1 > U_0$. This happens since the space-averaged Nusselt number is not dependent on the direction of the velocity, which changes as a result of the acoustic field, and is dependent only on the magnitude of the total flow velocity.

Figure 9 shows $Nu_s - 2$ at $Re_0 = 31.5$ and $Re_1 = 15.7$, 31.5, 62.9, 94.4, 157.3 for frequencies of 50, 1000 and 2000 Hz in order to determine the effect of frequency on the quasi-steady space-averaged Nusselt number. When $Re_1 < Re_0$ with $Re_0 = 31.5$ and $Re_1 = 15.7$ as shown in Fig. 9, the high peak value of U is 7.5 m s^{-1} at $\tau = 0$ and 1. The minimum value is 2.5 m s^{-1} at $\tau = 0.5$. $Nu_s - 2$ does not vary much with frequency. When $Re_1 = Re_0 = 31.5$, the low and high peak values of U over one cycle are, respectively, 0 and 10 m s^{-1} over one cycle. The high peak values of $Nu_s - 2$ are saturated but the low peak values increases with increasing frequency. With increasing acoustic Reynolds number for $Re_0 = 31.5$, when $Re_1 > Re_0$, the two high and low peak values of $Nu_s - 2$ exist within one cycle. Unlike the case without the convective velocity U_0, the values of U at around $\tau = 0$ are higher than those at around $\tau = 0.5$. The two low peaks have similar values which occur when $U = U_0 + U_1 \cos(2\pi\tau) = 0$. With increasing frequency and acoustic Reynolds number Re_1, the two

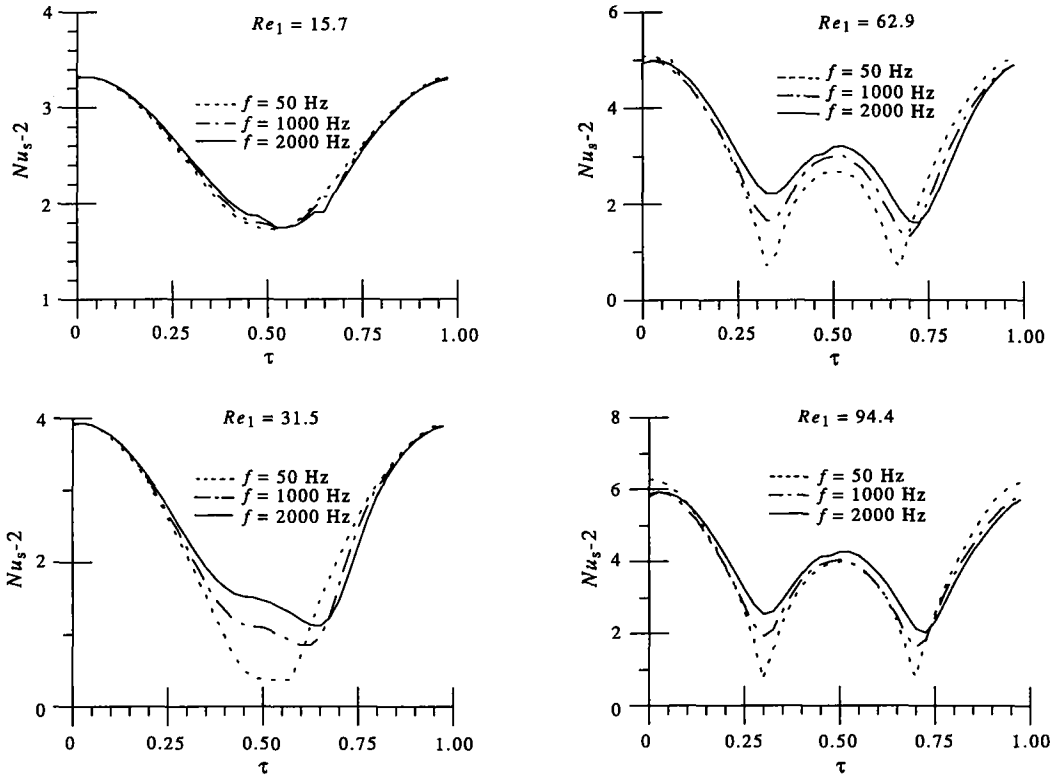

FIG. 9. Quasi-steady space-averaged Nusselt number for frequencies of 50, 1000 and 2000 Hz: $S = 0.00033-0.08$, $Re_0 = 31.5$, $Re_1 = 15.7$–94.4 ($SPL = 151$–167 dB).

high peak values are saturated and the two low peak values are increased, similar to the case without convective velocity as shown by Ha [14].

Figure 10 shows the space- and time-averaged quasi-steady Nusselt number (Nu_t-2), normalized by its steady flow value, as a function of the velocity ratio $\varepsilon(=(U_1/U_0)$ or $(Re_1/Re_0))$ in the Strouhal number range of 0.0001–0.08. As discussed earlier, with increasing frequency and acoustic Reynolds number Re_1, the two high peak values are saturated and the two low peak values are increased similar to the case without convective velocity. Therefore, as shown in Fig. 10, $(Nu_t-2)/(Nu_0-2)$ have slightly different values for different frequencies of 50, 1000 and 2000 Hz, with a maximum difference of 10%. There is an increase in $(Nu_t-2)/(Nu_0-2)$ with ε. For example, at $\varepsilon = 5$ the increase is about 85% compared to the case with no acoustic field. For much larger actual ε, the increase in $(Nu_t-2)/(Nu_0-2)$ is much more significant, approaching asymptotically the case of an oscillating flow with no steady component. However, for $0 \leqslant \varepsilon \leqslant 1$ the value of $(Nu_t-2)/(Nu_0-2)$ changes from 1.0 to around 0.9, meaning that there is a slight decrease in the Nusselt number when $U_1 < U_0$. The present prediction for $U_1 < U_0$ and 50 Hz (close to the case of the quasi-steady state) gives almost the same results as correlation obtained from the quasi-steady convection analysis by Mori *et al.* [3]. The maximum difference is about 2.5%. In general, increas-

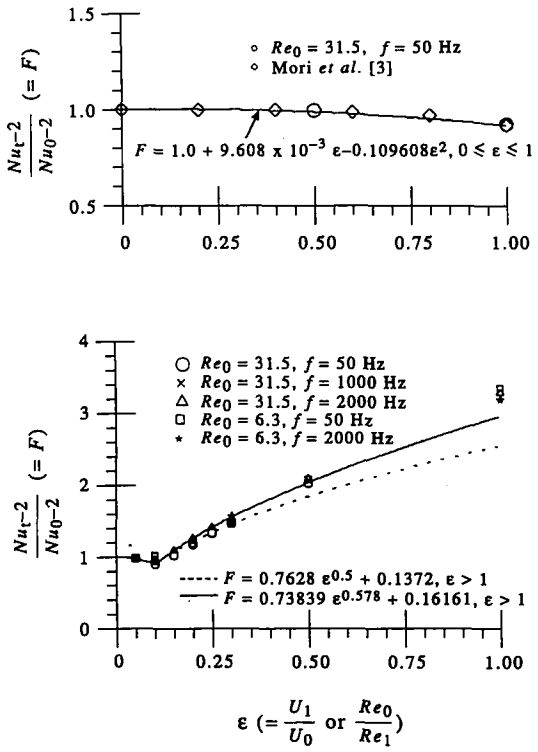

FIG. 10. Space- and time-averaged Nusselt number normalized by its steady value as a function of Reynolds number ratio.

ing the oscillating velocity superposed on a steady component creates a larger average slip velocity between the particle and surrounding gas, resulting in increased heat transfer as compared to the case of steady flow alone. This is generally the case for pulverized coal combustion and, the later stages of coal–water slurry fuel combustion.

Thus, with the acoustic field superposed on a steady flow velocity $U_0(|\mathbf{v}_g-\mathbf{v}_p|)$, the dimensionless space- and time-averaged, steady periodic state heat and mass transfer coefficient, normalized by their steady flow valucs, as a function of the ratio $\varepsilon(=(U_1/U_0)$ or $(Re_1/Re_0))$ for a spherical particle can be expressed as follows:

$$\frac{Nu_t-2}{Nu_0-2} \quad \text{or} \quad \left(\frac{Sh_t-2}{Sh_0-2}\right)=F(\varepsilon). \tag{9}$$

Using the results shown in Fig. 10 and those of refs. [3] and [5], F in equation (9) can be written as follows:

at $0 \leqslant \varepsilon \leqslant 1$,

$$F = 1.0+9.608\times 10^{-3}\varepsilon-0.109608\varepsilon^2 \tag{10}$$

and at $\varepsilon > 1$, for the dotted line in Fig. 10,

$$F = 0.7628\varepsilon^{0.5}+0.1372 \tag{11}$$

for the solid line in Fig. 10,

$$F = 0.73839\varepsilon^{0.578}+0.16161. \tag{12}$$

For small Strouhal numbers less than 0.1 and as $U_0 \to 0$ and $\varepsilon \to \infty$, the dotted line in equation (11) asymptotically approaches the following:

$$F = 0.7628\varepsilon^{0.5} \tag{13}$$

which is the same expression as given by Larsen and Jensen [5] and yields the expression for Nu_t-2 given by Ha [14]. The solid line in Fig. 10 approaches the following as $\varepsilon \to \infty$:

$$F = 0.73839\varepsilon^{0.578} \tag{14}$$

which is the same expression as given by Sayegh and Gauvin [15] and yields the expression for Nu_t-2 given by Ha [14].

SUMMARY AND CONCLUSIONS

The axisymmetric and laminar conservation equations for mass, momentum and energy for flow around a single spherical particle in the presence of an acoustic field are solved numerically with different values of the steady, acoustic Reynolds number and Strouhal number. The present simulation results compare well with the previously published results for the separation angle and the Nusselt number in the steady Reynolds number range of 10 to 100 without a superposed oscillating velocity ($Re_1 = 0$).

In the case of an oscillating flow superposed on a steady flow around a spherical particle, the following are the major findings of the present studies:

(1) If U_0 is greater than U_1 ($Re_0 > Re_1$), the flow is always in the direction of steady flow. The space-averaged Nusselt number shows the same cyclic behavior as the acoustic velocity U. There is asymmetry in Nu_s-2 during one cycle due to a favorable pressure gradient in the first half cycle and an adverse one in the following half cycle induced by the flow acceleration at infinity which changes the size of the separated region. The space-averaged Nusselt number increases with increasing frequencies due to an increase in the separated region. When $Re_1 > Re_0$, the two high and low peak values of the space-averaged Nusselt number are observed corresponding to the maximum and zero values of oscillating flow velocity U. Another high peak value of the space-averaged Nusselt number, which is less than the highest peak values, is observed at a half time of a period. The space-averaged Nusselt number shows an increase in the amplitude of the oscillation of Nu_s with increasing acoustic Reynolds number.

(2) Due to the combined effects of the differences in the time scales and of the flow separation caused by the flow acceleration, the normalized space- and time-averaged Nusselt number $(Nu_t-2)/(Nu_0-2)$ have slightly different values for different frequencies of 50, 1000 and 2000 Hz, with a maximum difference of 10%.

(3) The normalized space- and time-averaged Nusselt number $(Nu_t-2)/(Nu_0-2)$ changes from 1.0 to around 0.9 when the steady velocity U_0 is higher than the oscillating component U_1, indicating a slight decrease in heat transfer rate. When U_1 is larger than U_0, $(Nu_t-2)/(Nu_0-2)$ increases showing an enhancement of heat transfer rate. For example at $\varepsilon = 5$ the increase in $(Nu_t-2)/(Nu_0-2)$ is about 85% compared to the case with no acoustic field.

(4) Increases in the Nusselt number are more significant for larger acoustic velocities, which corresponds to the case of pulverized coal combustion and the later stages of coal–water slurry fuel combustion, under high intensity acoustic fields.

Acknowledgements—This work was supported by the U.S. Department of Energy, Morgantown Energy Technology Center, under contract DE-RA21-86MC23257.

REFERENCES

1. R. C. Marthelli and L. M. K. Boelter, The effect of vibration on heat transfer by free convection from a horizontal cylinder, *Proc. 5th Int. Congress of Applied Mechanics*, pp. 578–584 (1939).
2. C. B. Baxi and A. Ramachandran, Effect of vibration of heat transfer from spheres, *Trans. ASME, J. Heat Transfer* 337–344 (August 1969).
3. Y. Mori, M. Imabayashi, K. Hijikata and Y. Yoshida, Unsteady heat and mass transfer from spheres, *Int. J. Heat Mass Transfer* **12**, 571–585 (1969).
4. H. Gibert and H. Angelino, Transferts de matiere entre une sphere soumise a des vibrations et un liquide en mouvement, *Int. J. Heat Mass Transfer* **17**, 625–632 (1974).
5. P. S. Larsen and J. W. Jensen, Evaporation rates of

drops in forced convection with superposed transverse sound field, *Int. J. Heat Mass Transfer* **21**, 511–517 (1978).
6. S. A. Rawson, An experimental investigation of the influence of high intensity acoustics on heat and mass transfer rates from spheres as related to coal–water slurry fuel combustion enhancement, M.S. Thesis, The Pennsylvania State University, Pennsylvania (1988).
7. B. T. Zinn, J. R. Carvalho, Jr., N. Miller and B. R. Daniel, Pulsating combustion of coal in a rijke type combustor, *19th Symposium (International) on Combustion*, The Combustion Institute, pp. 1197–1203 (1982).
8. R. J. Faeser, Acoustic enhancement of pulverized coal combustion, ASME Paper 84-WA/NCA-18 (1984).
9. G. M. Koopmann, A. W. Scaroni, S. Yavuzkurt, G. Reethof, P. Ramachandran and M. Y. Ha, Acoustically enhanced combustion of micronized coal water slurry fuel, Final Report to DOE/METC under Contract No. DE-RA21-86MC23257, The Pennsylvania State University, Pennsylvania (May 1989).
10. S. Yavuzkurt, M. Y. Ha, G. M. Koopmann and A. W. Scaroni, A model of the enhancement of coal combustion using high intensity acoustic fields, *Proceedings on Heat Transfer Phenomena in Radiation, Combustion and Fires*, HTD-Vol. 106, pp. 439–446, ASME National Heat Transfer Conference (1989).
11. S. Yavuzkurt and M. Y. Ha, A model of the enhancement of the combustion of coal water slurry fuels using high intensity acoustic fields, *89-WA/NCA-2*, ASME Winter Annual Meeting (1989).
12. S. V. Patankar, *Numerical Heat Transfer and Fluid Flow* (1st Edn). Hemisphere, Washington D.C. (1980).
13. J. P. Van Doormaal and G. D. Raithby, Enhancement of the SIMPLE method for predicting incompressible fluid flow, *Numer. Heat Transfer* **7**, 147–163 (1982).
14. M. Y. Ha, A theoretical study of augmentation of particle combustion via acoustic enhancement of heat and mass transfer, Ph.D. Thesis, The Pennsylvania State University, Pennsylvania (1990).
15. N. N. Sayegh and W. H. Gauvin, Numerical analysis of variable property heat transfer to a single sphere in high temperature surroundings, *A.I.Ch.E. Jl* **25**(3), 522–534 (1979).